Turkish J. Eng. Env. Sci.
28 (2004) , 207 – 221.

Numerical Study of Wind-Induced Currents in Enclosed Homogeneous Water Bodies

Müsteyde Baduna KOÇYİĞİT, Önder KOÇYİĞİT
Gazi University, Faculty of Engineering, Ankara-TURKEY
e-mail: baduna@gazi.edu.tr

Received 09.02.2004

Abstract

Results of various circulation scenarios for wind-induced currents both in rectangular basins of constant depth and varying topography and in a small lake with a complex bathymetry are presented. The importance of some of the physical factors affecting the circulation pattern due to wind forcing in enclosed shallow homogeneous water bodies and the prediction of how physical changes might alter the circulation pattern were investigated. A 3-dimensional semi-implicit finite difference code was developed. The non-hydrostatic pressure component and the conventional sigma coordinate system in the vertical direction were incorporated into the model to take into account the effect of the vertical acceleration component and the bathymetric changes considered to be relatively important physical parameters for the circulation pattern. It was shown that the numerical model developed was capable of simulating wind-induced circulation in shallow enclosed water bodies and that the effect of topography and wind stress on the circulation pattern was of primary importance while the non-hydrostatic pressure component did not have much effect.

Key words: Wind-induced circulation, Non-hydrostatic pressure distribution, Shallow water, Sigma coordinate.

Introduction

In recent decades, an increasing practical interest in water circulation in reservoirs and lakes has arisen due to the problems of water quality encountered in these water bodies from where water is supplied for either domestic or industrial use. This interest has led to the development of many numerical models because of the unavailability of precise mathematical solutions to those problems of water quality. The formulation of the mathematical model in the coordinate system adapted is based on the physical properties of the flow domain and realistic assumptions (Koutitas and O'Connor, 1980). Hence, a large variety of numerical models have been developed over the years. In the early 1980s, 2-dimensional models which are computationally efficient and easily implemented were successfully used to predict the flow field and the distribution of pollutants (Falconer, 1986; Cheng *et al.*, 1993; Hayter *et al.*, 1997). However, it was soon recognised that the 2-dimensional models were not appropriate to simulate wind-induced circulation due to their incapability of describing the detailed structure of velocity and thereby simulating the 3-dimensional effects. Moreover, a bed stress calculation performed in 2-D models is physically unrealistic since bed stress cannot be adequately parameterised in terms of depth-averaged velocity. Consequently 3-dimensional models such as multilayer models (Falconer, 1993) and quasi-3D models (Koutitas and Gousidou-Koutita, 1986) have been developed, thus including vertical variations in the overall solution accuracy and producing variations in current and concentration through the vertical as well as in the horizontal. In order to increase the prediction capability of 3-D models, a large variety of numerical solution schemes (Simons, 1980; Sheng, 1994), orthogonal (Hamrick, 1994)

and non-orthogonal grid transformations (Borthwick and Barber, 1992), quad-tree mesh generation techniques (Bortwick *et al.*, 2001; Koçyiğit, 2003) and sub-structuring techniques (Wang and Hutter, 2000) have been developed over the years using various assumptions and simplifications.

The aim of this study was to develop a 3-dimensional numerical model capable of simulating the 3-dimensional effects of wind-induced currents and flow over complex bathymetry in enclosed water bodies and to predict how the physical changes might alter the circulation pattern. The non-hydrostatic pressure distribution was incorporated into the model equations to take into account the possible impact of vertical acceleration on the current structure and thus on the circulation pattern where complex bathymetric changes may cause such phenomena.

Mathematical Formulation

The mathematical model is based on the Reynolds-Averaged Navier-Stokes equations, which are derived using the principle of conservation of fluid mass and momentum. After resolving the pressure term into hydrostatic ($P_h = \rho g(\eta - z)$) and hydrodynamic ($P_{dyn} = q$) components and introducing the notation of the eddy viscosity coefficient, the momentum and continuity equations for an incompressible fluid can be expressed in a sigma coordinate system in a fully conservative form as

$$\frac{\partial(Hu)}{\partial t} + \frac{\partial(Huu)}{\partial x} + \frac{\partial(Hvu)}{\partial y} + \frac{\partial(\omega u)}{\partial \sigma} = fHv - Hg\frac{\partial \eta}{\partial x} - \frac{H}{\rho}\frac{\partial q}{\partial x} + H\frac{\partial}{\partial x}(\nu_h \frac{\partial u}{\partial x}) + H\frac{\partial}{\partial y}(\nu_h \frac{\partial u}{\partial y}) + \frac{\partial}{\partial \sigma}(\frac{\nu_v}{H}\frac{\partial u}{\partial \sigma}) \quad (1)$$

$$\frac{\partial(Hv)}{\partial t} + \frac{\partial(Hvu)}{\partial x} + \frac{\partial(Hvv)}{\partial y} + \frac{\partial(\omega v)}{\partial \sigma} = -fHu - Hg\frac{\partial \eta}{\partial y} - \frac{H}{\rho}\frac{\partial q}{\partial y} + H\frac{\partial}{\partial x}(\nu_h \frac{\partial v}{\partial x}) + H\frac{\partial}{\partial y}(\nu_h \frac{\partial v}{\partial y}) + \frac{\partial}{\partial \sigma}(\frac{\nu_v}{H}\frac{\partial v}{\partial \sigma}) \quad (2)$$

$$\frac{\partial(Hw)}{\partial t} + \frac{\partial(Hwu)}{\partial x} + \frac{\partial(Hwv)}{\partial y} + \frac{\partial(w\omega)}{\partial \sigma} = -\frac{1}{\rho}\frac{\partial q}{\partial \sigma} + H\frac{\partial}{\partial x}(\nu_h \frac{\partial w}{\partial x}) + H\frac{\partial}{\partial y}(\nu_h \frac{\partial w}{\partial y}) + \frac{\partial}{\partial \sigma}(\frac{\nu_v}{H}\frac{\partial w}{\partial \sigma}) \quad (3)$$

$$\frac{\partial \eta}{\partial t} + \frac{\partial(Hu)}{\partial x} + \frac{\partial(Hv)}{\partial y} + \frac{\partial(\omega)}{\partial \sigma} = 0 \quad (4)$$

where x, y and σ = sigma coordinates oriented eastward, northward, and upward, respectively; u, v = velocity components in the horizontal x- and y-directions while w, ω = velocity components in the vertical in Cartesian and sigma coordinates, respectively; η = water surface above horizontal datum (z = 0 at the undisturbed water surface); H = total depth of water column; q = non-hydrostatic pressure component; t = time; g = gravitational acceleration; ρ = fluid density; f = the Coriolis parameter; ν_h and ν_v = the kinematics eddy viscosity coefficients in the horizontal and vertical directions, respectively. The vertical eddy viscosity ν_v was represented using a 2-layer mixing length model (Rodi, 1984), while the horizontal eddy viscosity ν_h was either simply taken to be a constant value or represented by a Smagorinsky algebraic subgrid scale turbulence model (Wang, 1995) to include large scale turbulence effects generated by the horizontal shear. The new vertical velocityω, defined as $\omega = H(d\sigma/dt)$, is related to w by the following relationship

$$\omega = w - u(\sigma\frac{\partial H}{\partial x} + \frac{\partial \eta}{\partial x}) - v(\sigma\frac{\partial H}{\partial y} + \frac{\partial \eta}{\partial y}) - (\sigma\frac{\partial H}{\partial t} + \frac{\partial \eta}{\partial t}) \quad (5)$$

Another equation deployed in the current model is the well-known free surface equation, which is derived by integrating the continuity Eq. (4) in the vertical direction from $\sigma = -1$ to $\sigma = 0$ and substituting the kinematic boundary condition at the free surface and the no-slip boundary condition at the bed. After applying the Leibniz rule it can be written as

$$\frac{\partial \eta}{\partial t} + \frac{\partial}{\partial x}\left[H\int_{-1}^{0} u d\sigma\right] + \frac{\partial}{\partial y}\left[H\int_{-1}^{0} v d\sigma\right] = 0 \quad (6)$$

Equation (6) can be used to determine and advance the position of the free surface when all 3 components of the velocity at the surface are known (Jankowski, 1999). It should also be noted here that the horizontal gradients of the non-hydrostatic pressure q and the horizontal diffusion terms in momentum equations in Cartesian coordinates are not transformed into the sigma coordinate system in order to avoid large errors, especially near steep bottom slopes where small pressure gradients might be the result of the sum of 2 relatively large terms of opposite sign, resulting in a relatively large error in the pressure gradient that can induce artificial flows (Haney, 1991; Stelling and Van Kester, 1994). Details of the mathematical model and the governing equations can be found in Koçyiğit (2002).

Numerical Solution Method

A fractional step method, first proposed by Casulli and Cheng (1992) and then improved by Casulli and Stelling (1998), is used to solve the 3-dimensional free surface flow equations in 2 steps. For the first step the gradient of the surface elevation in the horizontal momentum equations and the horizontal velocities in the surface equation are discretised using the θ-method, with θ being an implicitness parameter. In the momentum equations, the vertical viscosity terms are discretised implicitly for stability, while the rest of the terms, i.e. the advection, Coriolis and horizontal viscosity terms, are discretised explicitly. The non-hydrostatic pressure is also included in the momentum equations for incorporating the effects of the hydrodynamic pressure distribution on the free-surface elevation. For the discretisation of the equations, a conventional staggered mesh system was used. The centre of the cells was numbered with indices i, j and k, where i = 1,...., I, j = 1, ..., J and k = 1, ..., K, with $k = 1$ for the surface cell and $k = K$ for the bed cell. The u-velocity was then defined at (i+1/2, j, k); the velocity v was defined at $(i, j + 1/2, k)$ and the vertical velocities w and ω were defined at the node $(i, j, k - 1/2)$. The hydrodynamic pressure term q was defined at the node (i, j, k), the surface elevation η was defined at the cell centre (i, j) and the water depth $H(x, y)$ was specified at the centre of each grid side, i.e. $(i+1/2, j)$ and $(i, j + 1/2)$, thereby providing a comprehensive representation of the bathymetry. Finally, σ represents the sigma value of a level and $\Delta\sigma$is the vertical mesh spacing in sigma coordinates. After discretisation of the horizontal momentum equations and substitution of the horizontal velocities from the discretised momentum equations into the discretised free surface equation, the free surface equation is obtained in the following form

$$
\begin{aligned}
&\eta_{i,j}^{n+1} \\
&-g\theta^2\frac{\Delta t^2}{\Delta x^2}\Big\{\big[(\Delta\sigma)^{\mathbf{T}}A^{-1}\Delta\sigma\big]^n_{i+1/2,j}(\eta_{i+1,j}^{n+1}-\eta_{i,j}^{n+1})-\big[(\Delta\sigma)^{\mathbf{T}}A^{-1}\Delta\sigma\big]^n_{i-1/2,j}(\eta_{i,j}^{n+1}-\eta_{i-1,j}^{n+1})\Big\} \\
&-g\theta^2\frac{\Delta t^2}{\Delta y^2}\Big\{\big[(\Delta\sigma)^{\mathbf{T}}A^{-1}\Delta\sigma\big]^n_{i,j+1/2}(\eta_{i,j+1}^{n+1}-\eta_{i,j}^{n+1})-\big[(\Delta\sigma)^{\mathbf{T}}A^{-1}\Delta\sigma\big]^n_{i,j-1/2}(\eta_{i,j}^{n+1}-\eta_{i,j-1}^{n+1})\Big\} \\
&=\delta_{i,j}^n-\frac{\Delta t}{\Delta x}\Big\{\big[(\Delta\sigma)^{\mathbf{T}}A^{-1}G\big]^n_{i+1/2,j}-\big[(\Delta\sigma)^{\mathbf{T}}A^{-1}G\big]^n_{i-1/2,j}\Big\} \\
&\quad-\frac{\Delta t}{\Delta y}\Big\{\big[(\Delta\sigma)^{\mathbf{T}}A^{-1}G\big]^n_{i,j+1/2}-\big[(\Delta\sigma)^{\mathbf{T}}A^{-1}G\big]^n_{i,j-1/2}\Big\}
\end{aligned}
\tag{7}
$$

where

$$
\delta_{i,j}^{n+1}=\eta_{i,j}^n-(1-\theta)\frac{\Delta t}{\Delta x}\left[\begin{array}{l}\sum\limits_{k=1}^{k=K}\Delta\sigma^n_{i+1/2,j,k}u^n_{i+1/2,j,k} \\ -\sum\limits_{k=1}^{k=K}\Delta\sigma^n_{i-1/2,j,k}u^n_{i-1/2,j,k}\end{array}\right]-(1-\theta)\frac{\Delta t}{\Delta y}\left[\begin{array}{l}\sum\limits_{k=1}^{k=K}\Delta\sigma^n_{i+1/2,j,k}\nu^n_{i,j+1/2,k} \\ -\sum\limits_{k=1}^{k=K}\Delta\sigma^n_{i,j-1/2,k}\nu^n_{i,j-1/2,k}\end{array}\right]
$$

and $G^n_{i+1/2,j}$and$G^n_{i,j+1/2}$contain all of the explicit terms, $A^n_{i+1/2,j}$and $A^n_{i,j+1/2}$contain the coefficients of the unknown velocities and $\Delta\sigma^n_{i+1/2,j}$and $\Delta\sigma^n_{i,j+1/2}$contain the layer thickness in the discretised momentum equations in x- and y- directions, respectively.

This 5-diagonal system of equations, with the unknowns $\tilde{u}^{n+1}_{i+1/2,j,k}$, $\tilde{v}^{n+1}_{i,j+1/2,k}$ (intermediate velocity field in the horizontal plane) and $\eta^{n+1}_{i,j}$ being specified over the entire computational mesh, has to be solved at each time step to determine recursively values of the field variables. Once the new surface elevation is determined, the discretised momentum equations are solved to determine the horizontal velocity field. If the model is run with the hydrostatic assumption, then the vertical velocity w at the new time level n+1 is to be found from the continuity equation. Otherwise the vertical momentum equation is used to determine the intermediate vertical velocity field.

In the second step the new velocity fields $u^{n+1}_{i+1/2,j,k}$, $v^{n+1}_{i,j+1/2,k}$ and $w^{n+1}_{i,j,k+1/2}$ are computed by correcting the intermediate velocity field ($\tilde{u}^{n+1}_{i+1/2,j,k}$, $\tilde{v}^{n+1}_{i,j+1/2,k}$ and $\tilde{w}^{n+1}_{i,j,k+1/2}$) with the gradient of the hydrodynamic pressure correction term, since the intermediate velocity field will not satisfy the local continuity equation. Hence, the hydrodynamic pressure correction term is determined by requiring that the new velocity field is convergent. Defining q′ as the hydrodynamic pressure correction term and satisfying the incompressibility condition in each computational grid, the following finite difference Poisson equation for the hydrodynamic pressure correction term is obtained as

$$\frac{\Delta t}{\Delta x^2}\Delta\sigma^n_{i+1/2,j,k}(q'^{n+1}_{i+1,j,k}-q'^{n+1}_{i,j,k})-\frac{\Delta t}{\Delta x^2}\Delta\sigma^n_{i+1/2,j,k}(q'^{n+1}_{i,j,k}-q'^{n+1}_{i-1,j,k})$$

$$+\frac{\Delta t}{\Delta y^2}\Delta\sigma^n_{i,j+1/2,k}(q'^{n+1}_{i,j+1,k}-q'^{n+1}_{i,j,k})-\frac{\Delta t}{\Delta y^2}\Delta\sigma^n_{i,j+1/2,k}(q'^{n+1}_{i,j,k}-q'^{n+1}_{i,j-1,k})$$

$$+\frac{1}{\Delta\sigma^n_{i,j,k-1/2}}(q'^{n+1}_{i,j,k-1}-q'^{n+1}_{i,j,k})-\frac{1}{\Delta\sigma^n_{i,j,k+1/2}}(q'^{n+1}_{i,j,k}-q'^{n+1}_{i,j,k+1})= \tag{8}$$

$$\frac{1}{\Delta x}\Big[\Delta\sigma^n_{i+1/2,j,k}\tilde{u}^{n+1}_{i+1/2,j,k}-\Delta\sigma^n_{i-1/2,j,k}\tilde{u}^{n+1}_{i-1/2,j,k}\Big]+\frac{1}{\Delta y}\Big[\Delta\sigma^n_{i,j+1/2,k}\tilde{v}^{n+1}_{i,j+1/2,k}-\Delta\sigma^n_{i,j-1/2,k}\tilde{v}^{n+1}_{i,j-12/,k}\Big]$$

$$+\Big[\tilde{w}^{n+1}_{i,j,k-1/2}-\tilde{w}^{n+1}_{i,j,k+1/2}\Big]$$

Thus, Eq. (8) forms a 7 diagonal linear system and can be solved iteratively by the conjugate gradient method. Once the hydrodynamic pressure correction term is computed, the final velocity field at the new time level can be determined from momentum equations and then the hydrodynamic pressure fields are updated with the hydrodynamic pressure correction term.

The system of equations is subject to various types of boundary conditions. At the solid impermeable boundaries, no mass flux is allowed through the boundary and therefore zero normal flow is imposed in momentum equations. At the surface, the hydrodynamic pressure q is set to zero, so a Dirichlet type of boundary condition is specified. For the case of a wind stress on the surface, the shear stress at the free surface is taken equal to the wind stress. An impermeability condition was implemented at the solid and lateral boundaries for velocity components with a Neumann boundary condition at the free surface in the presence of wind shear, taking $\omega = 0$ at the free surface and at the bed.

Since the θ-method is used in the model, it is important to choose the value of θ to be used in the numerical model. When $\theta = 1$, the algorithm becomes fully implicit and wave damping problems may arise. In order to avoid wave damping and to have high accuracy and efficiency, a semi-implicit scheme is used where $\theta = 1/2$, so that the average values of the pressure gradient and the velocities are used in the free surface and momentum equations. Details of the stability analysis, the accuracy and the efficiency of the method can be found in Casulli and Cattani (1994).

Model Verification and Application

Comparison with analytical solutions

The small amplitude wave test case was first performed to test mass and energy conservation and to demonstrate the effects of hydrodynamic pressure on the circulation pattern (Jankowski, 1999). For this test, a uni-nodal standing wave was simulated in a closed basin containing an inviscid fluid of constant water depth and density. A zero initial velocity was assumed and the initial free surface elevation was given by a half cosine curve. Comparisons of model predictions with analytical solutions were performed for free surface elevation, velocity field and hydrodynamic pressure distribution in the vertical section of the basin and presented for the same phases of motion of t = 3T/8 in Figure 1. The comparisons showed very good agreement between the analytical solutions and the numerical results. It was also shown in Figure 2 that the model with the hydrostatic approximation yielded long-wave velocity profiles, which were not realistic and physically not correct, compared to the physically correct and smooth velocity profiles obtained using the non-hydrostatic pressure algorithm. Details of the small amplitude wave theory, its analytical solution and the test case can be found in Jankowski (1999) and Koçyiğit (2002).

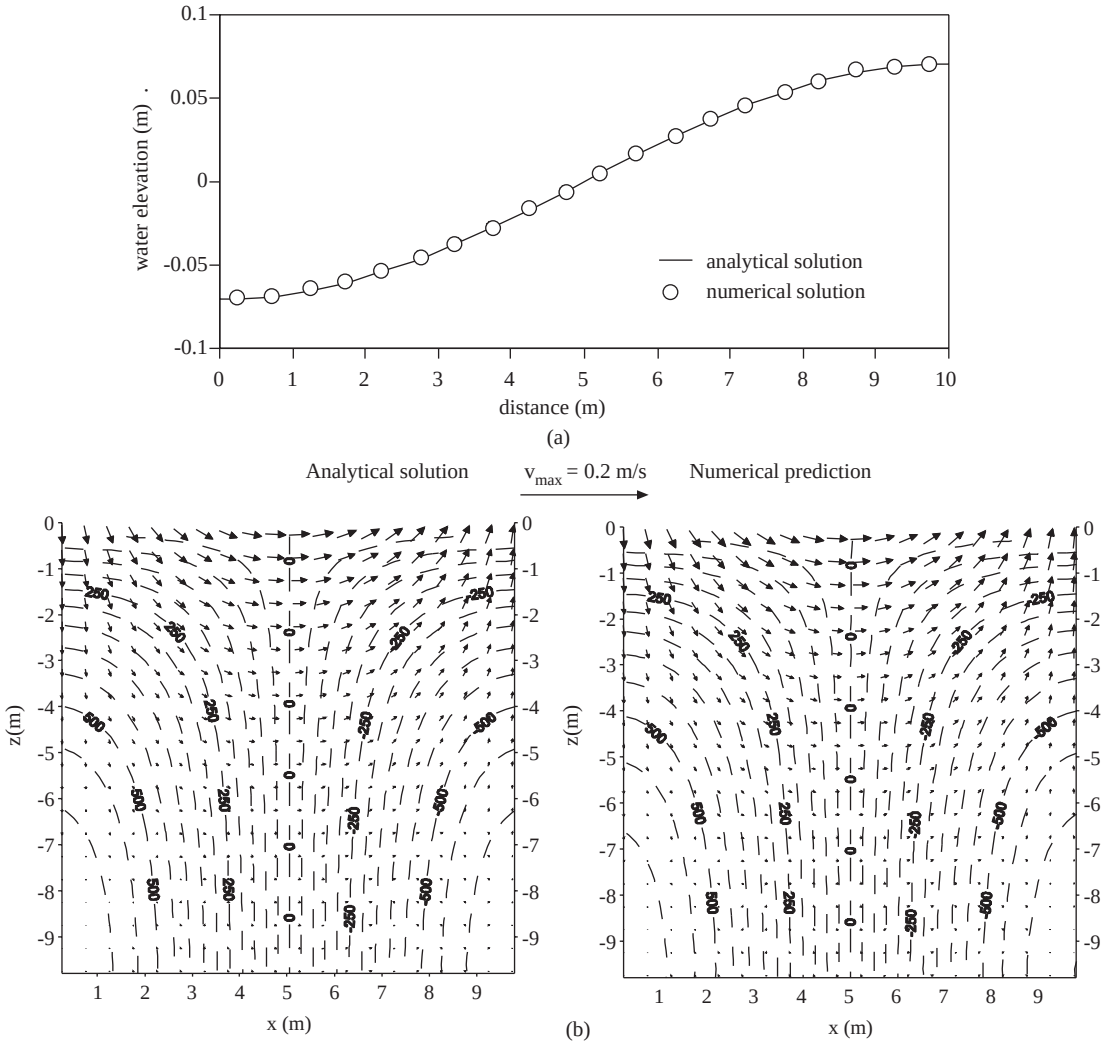

Figure 1. Comparison between numerical and analytical solutions for phase angle of t = 3T/8 for (a) free surface elevation; (b) velocity and hydrodynamic pressure fields in the vertical section (iso-lines of hydrodynamic pressure shown each 50 Pa).

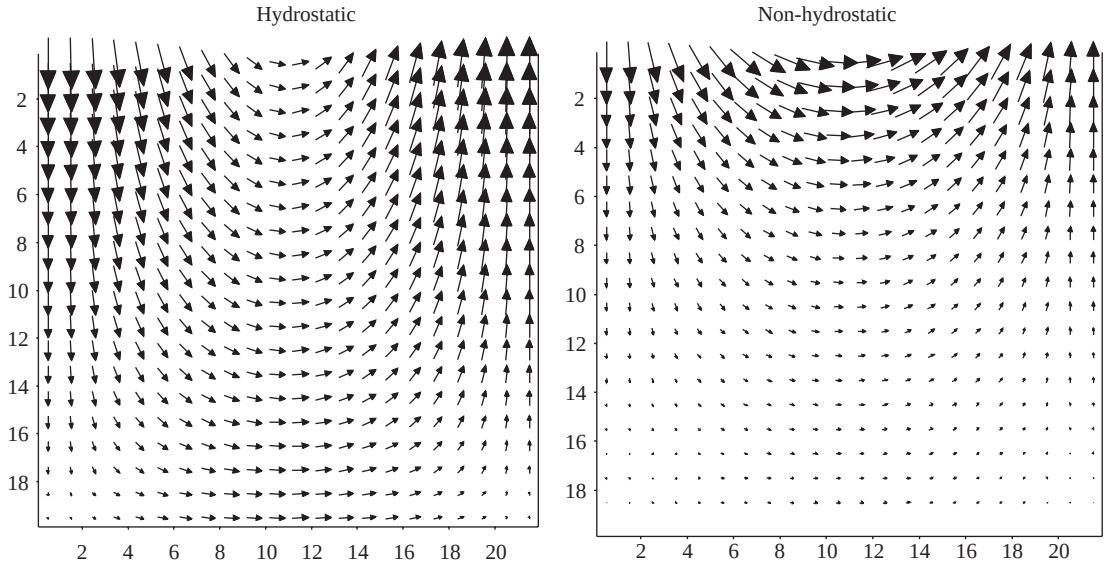

Figure 2. Comparison of solutions at T/4, both with and without hydrostatic approximation.

Another comparison of the model predictions to an analytical solution was performed for a steady wind-driven circulatory flow in a closed basin with a flat bed and linearised bottom friction (Huang, 1995). The test basin was square with an area of 12 km x 12 km and contained water 40 m deep. The advection, Coriolis, horizontal diffusion and cross (y-direction) terms were neglected, leading to a balance between the surface gradient, the vertical diffusion of momentum, the surface wind stress and the bottom friction term in the momentum equation. For this test case 2 wind conditions were applied, where the wind stress τ_w was set to 0.1 N/m^2 and 0.325 N/m^2, respectively. The model was started with a zero velocity field and elevation and the simulation continued under constant wind forcing. Numerical simulations were first carried out with an equal layer thickness over the water depth and then the grid resolution was enhanced near the surface and bottom boundaries, where steep velocity gradients were expected due to the wind and bed shear stresses. Comparisons of model predictions at the centre of the basin with the analytical solution for W = 5 m/s and W = 10 m/s for the case of evenly distributed layers are shown in Figure 3, where it can be seen that, as expected, the upper layer currents are in the wind direction while the lower layer currents are in the opposite direction, to maintain mass balance in the closed basin. Figure 4 shows the numerical model predictions at the centre of the basin for 5 and 10 layers, where the resolution near the surface and bed was enhanced using a number of logarithmic distributions of layers and with evenly distributed layers. The absolute error results showed that the model predictions approached the analytic solution both when the number of layers was increased and when the layers were concentrated near the boundaries. For the case of evenly distributed layers, the predictions improved by up to 82% for the velocity in the first layer near the surface and 70% for the velocity near the bed, with the number of layers increasing from 5 to 10 and from 5 to 16, respectively. For the case of a logarithmic distribution of layers, a higher accuracy was obtained, especially for the velocity near the bed. For instance an improvement of up to 95% was obtained for the case of an increase in the number of layers from 5 to 16. Details of the analytic solution for a constant vertical eddy viscosity and linearised bottom friction can be found in Huang (1995).

Verification using experimental data

A number of laboratory studies were carried out to measure wind-driven currents in experimental apparatus such as wind channels. One such laboratory work was performed by Tsuruya *et al.* (1985), whose experimental apparatus consisted of a wind-wave tank with a constant depth of 0.15 m and a length of 22 m. Some of the experimental parameters adopted are shown in Table 1. Two wind conditions, i.e. 6.73 m/s and 6.90 m/s, were used in the experiments. A comparison of the results of numeri-

cal model and experimental data is plotted in Figure 5. It can be observed that there was a noticeable agreement between the model simulations and the experimental data and that the numerical model is capable of simulating wind-induced current.

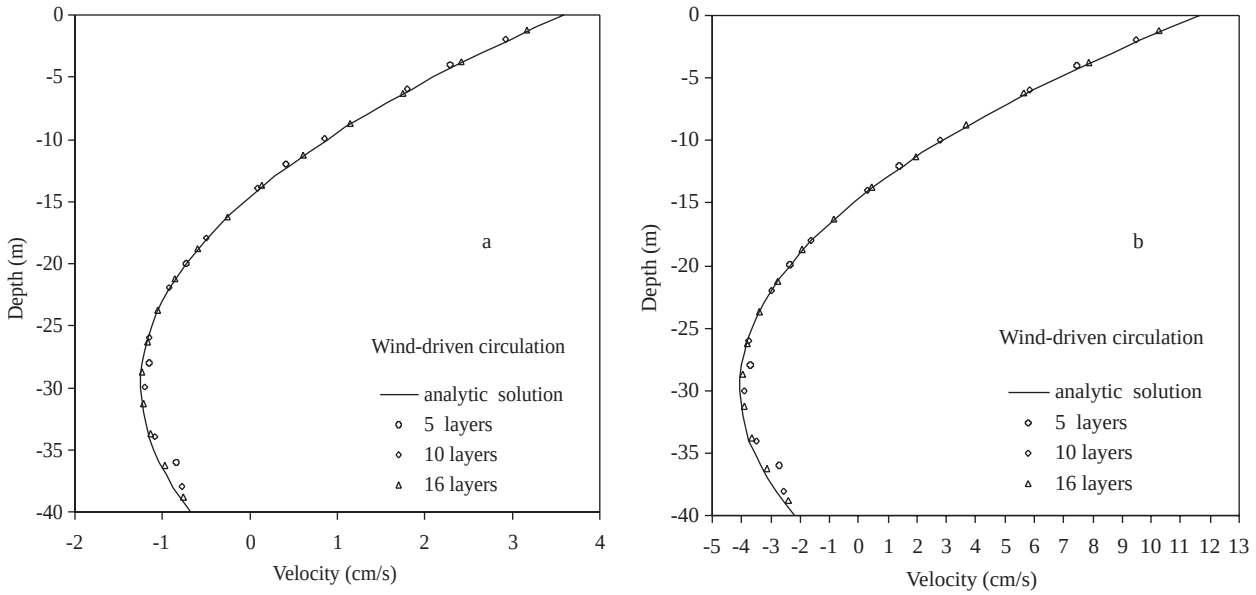

Figure 3. Comparison of numerical model predictions with analytical solution in the case of evenly distributed layers for: (a) W = 5 m/s, (b) W = 10 m/s.

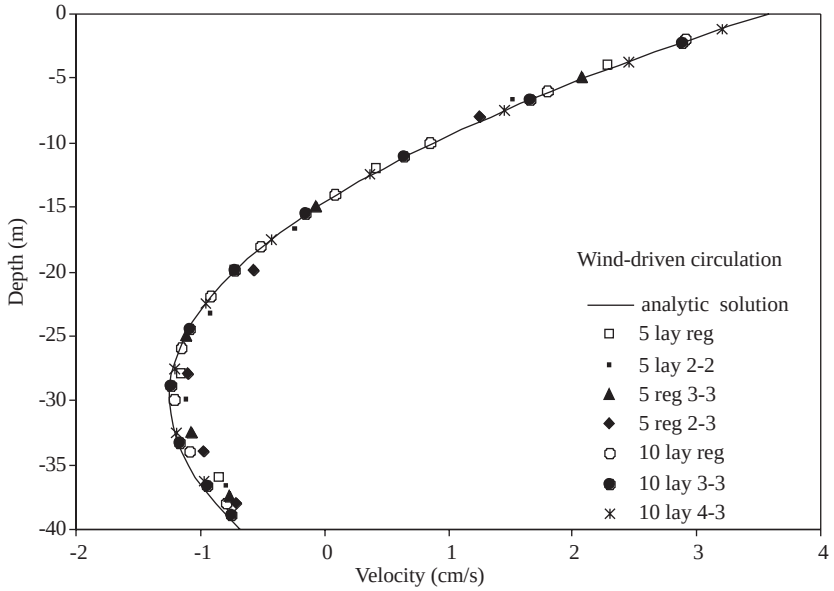

Figure 4. Comparison of numerical model predictions with analytical solution for evenly and various logarithmically distributed layers for W = 5 m/s ('lay' = layer; 'reg' = evenly distributed layers; '4-3' = higher resolution near surface (4 layers) and near bed (3 layers)).

Table 1. Experimental parameters and results from Tsuruya *et al.* (1985).

Quantity		Test1	Test2
(1)	(2)		
Depth	H (m)	0.15	0.15
Wind velocity	W (m/s)	6.90	6.80
Surface shear velocity	U_{*s} (cm/s)	0.815	0.835
Surface velocity	U_s (cm/s)	10.70	12.15
Reynolds number	R_s=u_sh/ν	16050	18225
Normalised surface velocity	U_s/u_{*s}	12.74	14.55
Absolute roughness	Z_{ow} (mm)	0.21	0.36

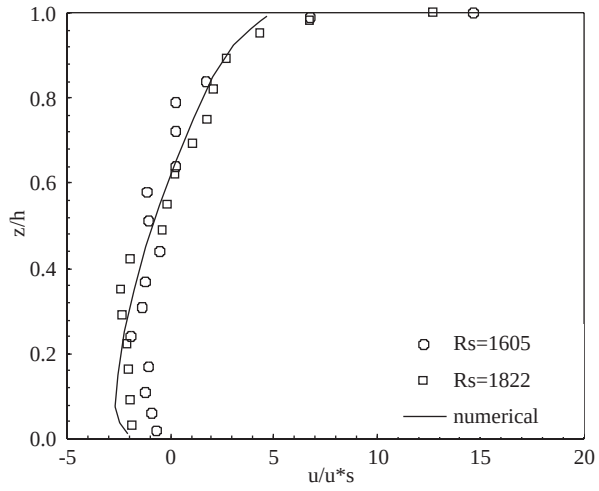

Figure 5. Normalised velocity profiles: verification of 3D model with experimental data (Tsuruya *et al.*, 1985).

Test cases under realistic conditions

The numerical model was then applied to 2 idealised rectangular basins, with sizes close to those of a typical lake and with different bathymetric layouts to demonstrate the model's 3-dimensional predictive capacity and to investigate the influence of the bathymetry on the wind-induced circulation patterns. One of the basins (Basin A) had a constant depth while the other (Basin B) had a depth varying bathymetry, as shown in Figure 6. The length (along the northern direction) and the width (along the eastern direction) of the basins were assumed to be 2.35 km and 0.85 km, respectively, while the depth was set to 15 m. A westerly wind of 5 m/s, blowing from west to east, was introduced in both basins and the predicted velocity fields at various layers are illustrated in Figure 7 after steady-state conditions had been reached. As seen in Figures 7a and b, there is a striking difference in the predicted circulation pattern, demonstrating the influence of the bathymetry on the velocity field across the basin. Two symmetric gyres, one clockwise and one anticlockwise, formed in Basin B due to the bathymetry, whereas in Basin A no such pattern was observed.

Application to a small lake

As a practical case study, Esthwaite Water, a small but morphometrically complex shallow lake in Cumbria, UK, was chosen to assess the model's capability of simulating the circulation patterns in a lake. Esthwaite Water has approximate dimensions of 2.3 km along the main axis, with a maximum width of 0.6 km and a maximum depth of nearly 16 m. A programme of field measurements was undertaken by Hall (1987) and took place during periods when the lake was in an isothermal state. Horizontal velocity profiles over the depth at many locations for wind conditions that would produce a near steady-state circulation pattern were obtained. Details about the lake, the field study and the measurement techniques

used can be found in Hall (1987). The numerical model was set up for Esthwaite Water and then the predictions were compared with measured velocity profiles at selected measurement sites in the lake. Figure 8 presents comparisons between the predicted and measured velocity profiles at one site in open water for a 3 m/s wind where generally an agreement is observed. Comparisons for a wind speed of 2.5 m/s are presented in Figure 9, with the numerically predicted currents being slightly lower than the measured currents. Stronger velocity components were reported along the wind axis while the slower velocity components were across the wind axis. This result suggested that the Coriolis force was influential in this small lake. However, comparisons in Figure 9 also showed that lateral boundaries affected the currents in these near-shore regions, where the Coriolis force was not effective and the continuity requirement generated a strong return current. The headlands and shoreline had a pronounced effect on the current structure, which was not well represented in the model. To improve on the predictions of the complex flow structure in the shallower regions close to the shore a finer horizontal mesh, which can be generated by an automatic mesh generation technique, is planned to be incorporated into the model at a later stage.

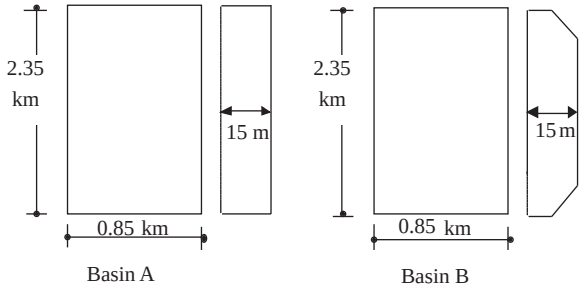

Figure 6. Simplified rectangular basins and their topography.

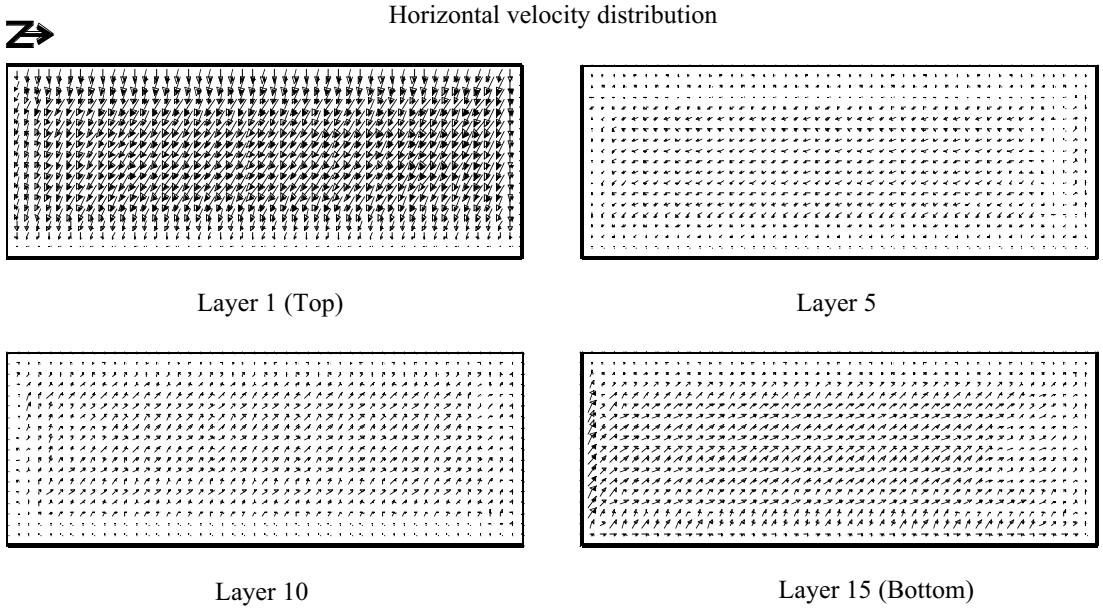

Figure 7a. Predicted circulation pattern in Basin A.

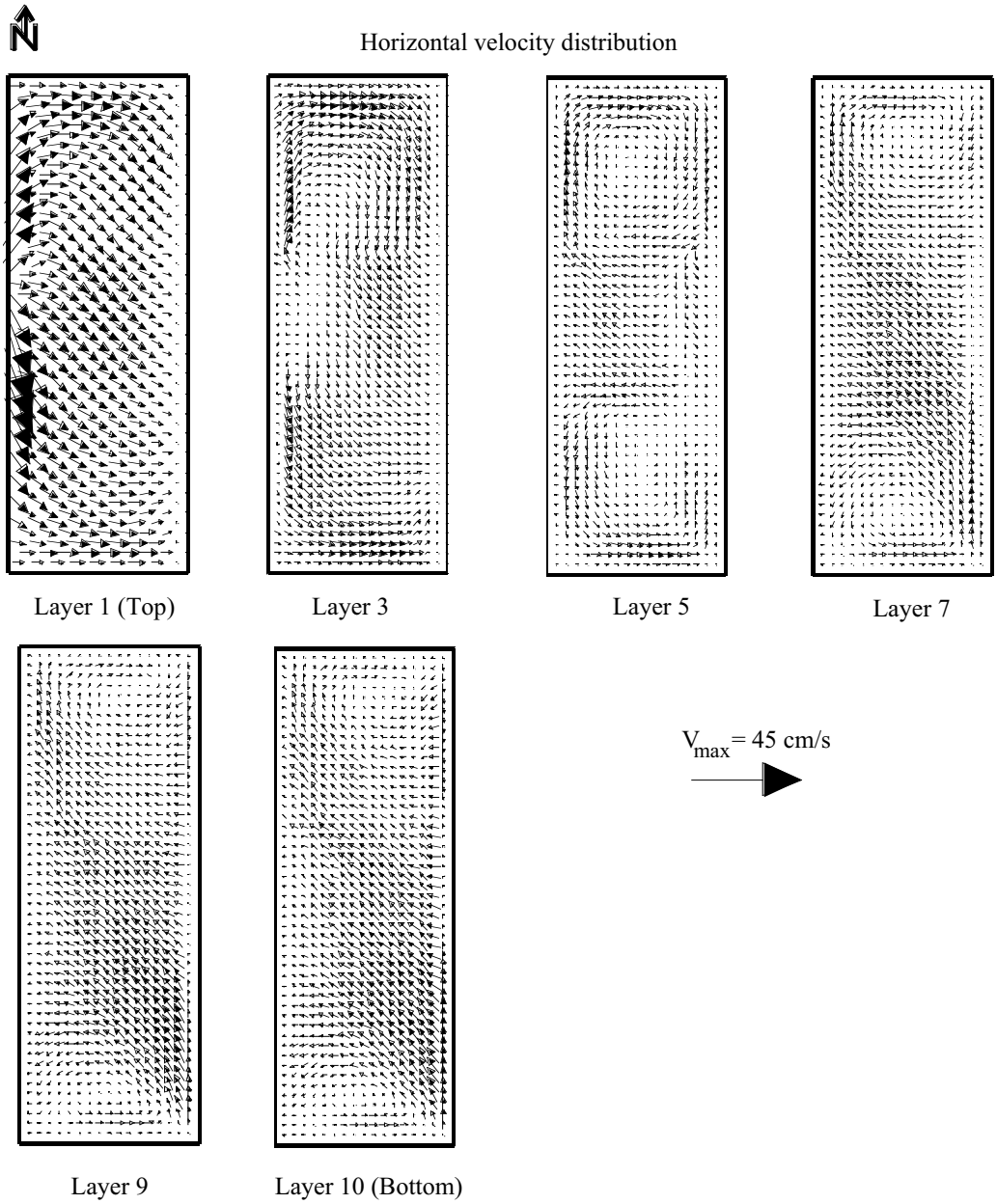

Figure 7b. Predicted circulation pattern in Basin B.

A series of simulations were also undertaken to examine the effect of several main model parameters on the circulation pattern across the entire lake and on the current structure over depth. The main parameters considered to have a pronounced effect on the circulation were eddy viscosity, wind speed, wind direction and bed roughness. Besides main parameters, the air-water resistance coefficient and the hydrodynamic pressure component were also investigated.

Firstly, a range of constant eddy viscosity coefficients and several turbulence models– of the 1 and 2 equation types– were deployed to predict the distribution of the vertical eddy viscosity coefficient. Numerical simulations showed that the eddy viscosity coefficient is of considerable importance in predicting the 3-dimensional velocity structure of wind-induced circulation and that the more sophisticated turbulence models deployed did not produce any improvements in the results when compared to a sim-

ple turbulence model, as shown in Figure 10. It has been noted previously by various researchers such as Koutitas and O'Connor (1980) and Tsanis (1989) that for wind-induced flows the accuracy of the numerical model results does not necessarily improve when more sophisticated turbulence models are deployed. The abbreviations used in the figure are as follows: 'tlml' = 2 layer mixing length model; 'cev' = constant eddy viscosity; 'k-lu' = 1-equation model; 'k-e' = 2-equation model and 'pedvl' = parabolic distribution of vertical eddy viscosity. In this study, the 2 layer mixing length model was chosen because of its easy implementation and low computational cost to provide an acceptable level of accuracy.

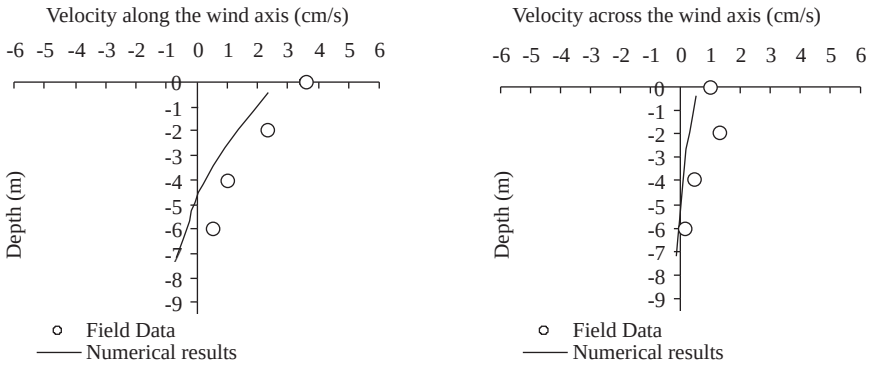

Figure 8. Predicted and measured velocity profiles at 2 sites in open water.

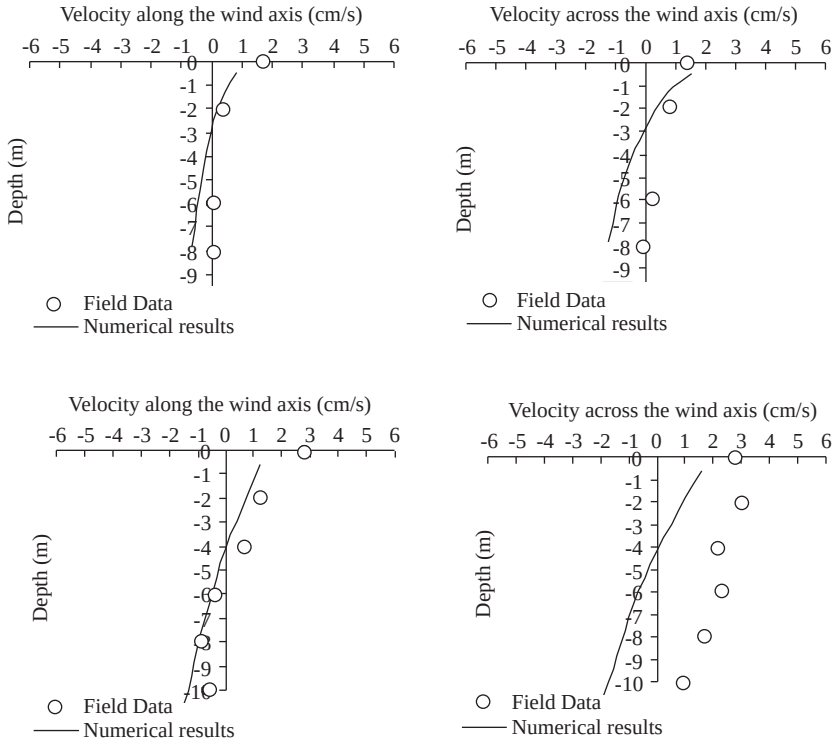

Figure 9. Predicted and measured velocity profiles at 2 sites in sheltered water.

As expected, the wind speed and wind direction were also found to have a significant impact on circulation since wind speed is directly proportional to the amount of energy put into the system. It was observed that the magnitude of the velocity field proportionally increased with increasing wind speed and that the size and location of eddies predicted changed noticeably with the wind direction.

Although the effect of Coriolis acceleration in small lakes is usually inferred to be negligible, field observations and numerical simulations presented in Figure 11 show that the current deflections in Esthwaite Water were significant where the surface layer velocities were deflected to the right of the wind direction for the case with the Coriolis acceleration being included and therefore it has a noticeable effect on the circulation patterns. This effect can especially be observed in the north-western bay of the lake.

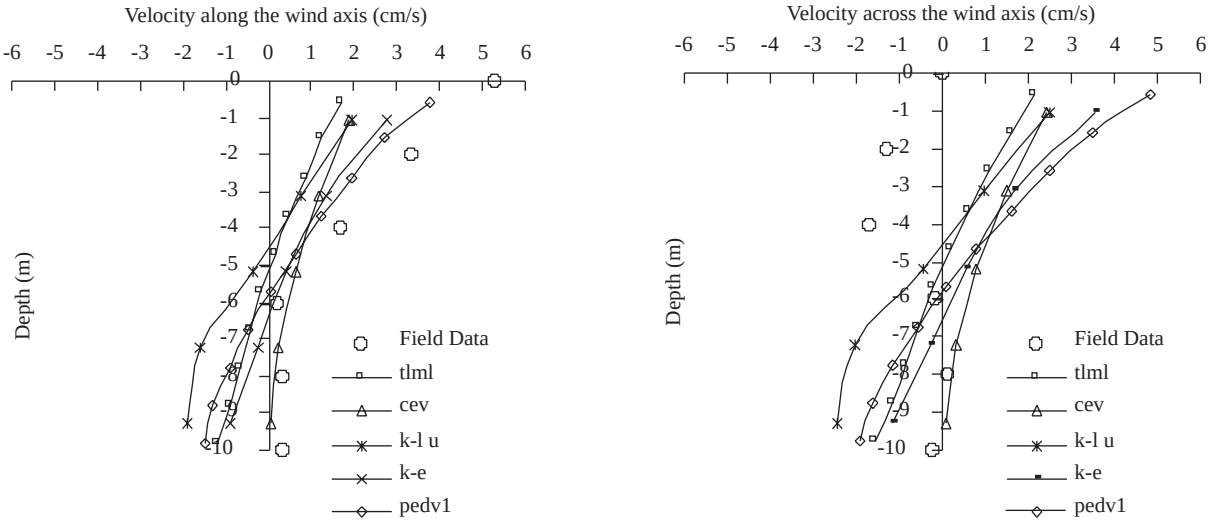

Figure 10. Comparison between measured and predicted velocities.

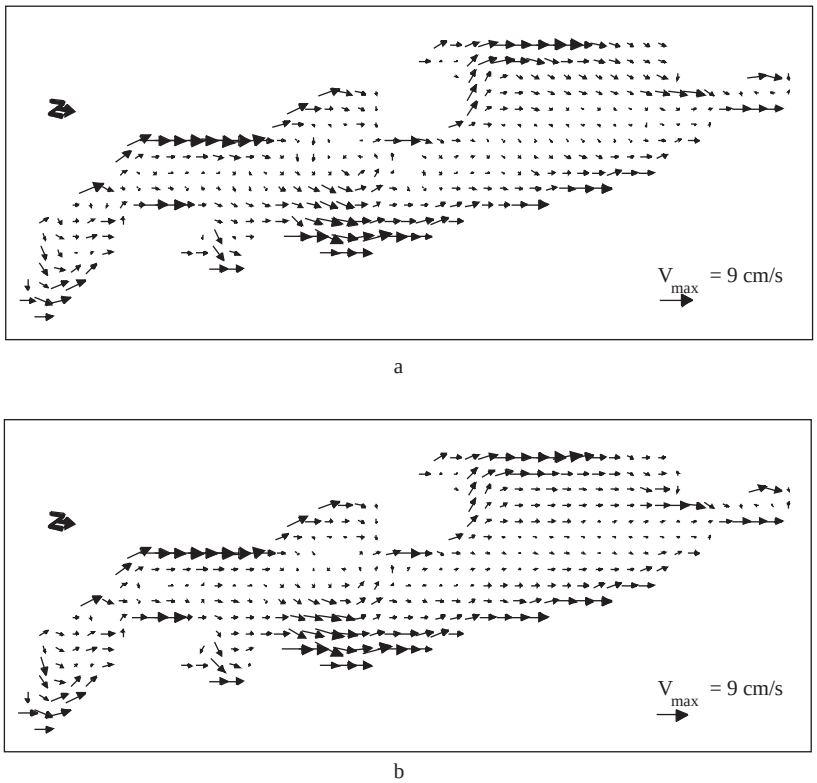

Figure 11. Predicted horizontal velocity field for surface layer with a wind speed of 3 m/s (a) including the Coriolis acceleration (b) neglecting the Coriolis acceleration.

The air-water resistance coefficient is another important parameter of wind-induced circulation as it affects the magnitude of the surface wind stress. Although a constant value of 2.6×10^{-3} was used in the simulations, numerous research studies showed that the value of this resistance coefficient depends upon many parameters, but mainly wind speed. A variety of formulations (Deacon and Webb, 1962; Wu, 1982; WAMDI, 1988) were tested and simulations showed that the proposed equations in the literature are usually inaccurate for lakes and other inland water bodies, where the wind speed may be affected by surrounding topography, thus leading to underestimated surface fluid velocities. In recent years research has been conducted on including coupled air-water models to hydrodynamic numerical models, where the influence of sheltering effects and the air-water resistance coefficient on the wind field can be included in the numerical model (Jinxiu *et al.*, 1999; Yang *et al.*, 2001).

The effect of the hydrodynamic pressure component on the circulation patterns across the entire lake and on the velocity structure at several sites was also investigated by comparing the measured and predicted profiles of the horizontal velocities. Although no visible effect of the hydrodynamic parameter on the overall circulation pattern in the lake was seen, a slight difference was observed in the velocity profile along the wind axis. For instance, for a wind speed of 7 m/s, the root mean square values for velocity along and across the wind axis were found to decrease from 10% to 6% and from 5.1% to 2.3%, respectively, at one site close to shore while a smaller decrease of 2% was computed at another site nearby. Therefore further comparisons with various data sets measured in steep sloped regions are essential for a clearer understanding of the effect of hydrodynamic pressure on the velocity profile.

Conclusions

A 3-dimensional numerical model has been developed to simulate wind-induced circulation in enclosed shallow homogeneous water bodies such as lakes and reservoirs and to interpret the importance of some of the physical factors affecting the circulation patterns due to wind forcing. The model was tested against available analytical solutions and laboratory data from the literature. It was shown that there was a very good agreement between the analytical solutions and the numerical model predictions, with the velocity structure over depth being well reproduced. Comparisons with laboratory data also showed that the model was capable of simulating wind-induced currents. A number of simulations were performed in idealised rectangular basins with different bathymetric layouts and it was observed that the bathymetry has a pronounced effect on the circulation patterns. Finally, the numerical model was applied to a shallow small lake. Simulations showed that the eddy viscosity coefficient, the wind speed and the wind direction are the main parameters affecting circulation and also that the Coriolis acceleration had a noticeable effect on the circulation patterns, except for close to lateral boundaries. It was also observed that the hydrodynamic pressure component had no visible effect on the overall circulation pattern with only a slight difference in the velocity profile along the wind axis. Further developments to the model would be to include the effects of lateral boundaries, thereby improving the shoreline representation, and to perform a wider range of field measurement programmes in regions close to the shore. The numerical model should also be applied to other shallow lakes for further investigation of the circulation patterns, sensitivity of the model parameters and calibration and validation of the model.

Acknowledgements

The authors are grateful to the Institute of Freshwater Ecology, for originally providing the hydrodynamic data for a Natural Environment Research Council CASE studentship. The authors also wish to thank Dr. D. G. George from the IFE, for his assistance in providing the data.

References

Borthwick, A.G.L., Cruz León, S. and Józsa, J., "Adaptive Quad-Tree Model of Shallow-Flow Hydrodynamics", Journal of Hydraulic Research, 39, 413-424, 2001.

Borthwick, A.G.L. and Barber, R.W., "River and Reservoir Flow Modelling Using the Transformed Shallow Water Equations", International Journal for Numerical Methods in Fluids, 14, 1193-1217, 1992.

Casulli, V. and Stelling, G.S., "Numerical Simula-

tion of Three Dimensional, Quasi-Hydrostatic Free-Surface Flows", ASCE Journal of Hydraulic Engineering, 124, 678-686, 1998.

Casulli, V. and Cattani, E., "Stability, Accuracy and Efficiency of a Semi-Implicit Method for Three Dimensional Shallow Water Flow", Computers Math. Application, 27, 99-112, 1994.

Casulli, V. and Cheng, R.T., "Semi-Implicit Finite Difference Methods for Three-Dimensional Shallow Water Flow", International Journal for Numerical Methods in Fluids, 15, 629-648, 1992.

Cheng, R.T., Casulli, V. and Gartner, J.W., "Tidal, Residual, Inter-Tidal Mudflat (TRIM) Model and Its Applications to San Francisco Bay, California", Estuarine, Coastal and Shelf Science, 36, 235-280, 1993.

Deacon, E.L. and Webb, K.E., "Interchange of Properties between Sea and Air: Small Scale Interactions", The Sea Vol. 1 (ed. Hill, M.N.) Inter science, New York, London, 1962.

Falconer, R.A., "An Introduction to Nearly Horizontal Flows", in Coastal, Estuarial and Harbour Engineers Reference Book (ed. Abbott, M.B. and Price W.A., F.N. Spon Ltd., London, 27-36, 1993.

Falconer, R.A., George, D.G. and Hall. P., "Three-Dimensional Numerical Modelling of Wind-Driven Circulation in a Shallow Homogeneous Lake", ASCE Journal of Hydrology, 124, 59-79, 1991.

Falconer, R.A., "Water Quality Simulation Study of a Natural Harbour", Journal of Waterway, Port, Coastal and Ocean Engineering, 112, 15-34, 1986.

Gaarthuis, J., "A Non-Hydrostatic Pressure Model for Shallow Water Flow: Analysis and Application of Three Methods to Compute a Non-Hydrostatic Correction Term", PhD Thesis, Technische Universiteit, Eindhoven, 1995.

Hall, P., "Numerical Modelling of Wind-Induced Lake Circulation", PhD Thesis, University of Birmingham, 292, 1987.

Hamrick, J., "A Three-Dimensional Model of Turkey Creek and Adjacent Indian Lagoon, Technical Report, Virginia Institute of Marine Science, 1994.

Haney, R.L., "On the Pressure Gradient Force over Steep Topography in Sigma Co-ordinate Ocean Models", AMS Journal of Physical Oceanography, 21, 610-619, 1991.

Hayter, E.J., Bergs, R. G. and McCutcheon, S.C., "HSCTM-2D, a Finite Element Model for Sediment and Contaminant Transport", Draft Report, U.S. Environmental Protection Agency, Athens, GA, 1997.

Huang, W. and Spaulding, M., "3D Model of Estuarine Circulation and Water Quality Induced by Surface Discharges" ASCE Journal of Hydraulic Engineering, 121, 300-311, 1995.

Jankowski, J.A., "A Non-Hydrostatic Model for Free Surface Flows", PhD Thesis. Hannover University, Germany, 1999.

Jinxiu, L., Shukun L., Shujun, L. and Xuezhong, Y., "Numerical Modelling of Wind-Induced Currents in Shallow Lakes", Environmental Hydraulics, (ed. Lee, Jayawardena and Wang) 1999.

Koçyiğit, Ö., "Modelling of Water Quality and Sediment Transport in Aquatic Basins Using an Unstructured Grid System", PhD Thesis. Cardiff University, Cardiff, UK, 2003.

Koçyiğit, M.B., "Numerical Modelling of Wind-Induced Circulation in Lakes and Reservoirs", PhD Thesis. Cardiff University, Cardiff, UK, 2002.

Koutitas, C. and Gousidou-Koutita, M., "A Comparative Study of Three Mathematical Models for Wind-Generated Circulation in Coastal Areas", Coastal Engineering, 10, 127-138, 1986.

Koutitas, C. and O'Connor, B., "Modelling Three-Dimensional Wind-Induced Flows", ASCE Journal of Hydraulic Division, 106, 1843-1865, 1980.

Rodi, W., Turbulence Models and Their Applications in Hydraulics, Delft: IAHR Publication, 1984.

Simons, T.J., "Circulation Models of Lakes and Inland Seas", Canadian Bulletin of Fisheries and Aquatic Sciences, Bulletin 203, Department of Fisheries and Oceans, Ottawa, 1980.

Sheng, Y.P., "Modelling Hydrodynamics and Water Quality Dynamics in Shallow Waters", Keynote Paper, Int. Symp. On Ecology and Engineering, Taman Negara, Malaysia, Nov. 1-4, 1994.

Stelling, G.S. and Van Kester, J.A.T.M., "On the Approximation of Horizontal Gradients in Sigma Co-ordinates for Bathymetry with Steep Bottom Slopes", International Journal for Numerical Methods in Fluids, 18, 915-935, 1994.

Tsanis, I.K., "Simulation of Wind-Induced Water Currents", ASCE Journal of Hydraulic Engineering, 115, 1113-1134, 1989.

Tsuruya, H., Nakamo, S. and Kato, H., "Experimental Study on Wind Driven Current in a Wind-Wave Tank-Effect of Return Flow on Wind-Driven Current", The Ocean Surface, 425-430, 1985.

WAMDI Group, "The WAM Model–A Third Generation Ocean Wave Prediction Model", Journal of Physical Oceanography, 18, 1775–1810, 1988.

Wang, H., Numerical Modeling of Flow and Disinfection Processes in Chlorine Contact Tanks, PhD Thesis, University of Bradford, UK, 1995.

Wang, Y. and Hutter, K., "Methods of Sub-Structuring in Lake Circulation Dynamics", Advances in Water Resources, 23, 399-425, 2000.

Wu, J., "Wind-Stress Coefficients over Sea Surface from Breeze to Hurricane", Journal of Geophysical Research, 87, 9704–9706, 1982.

Yang, J.S., Huang, W.G. and Zhou, C.B., "Retrieval of Ocean Surface Wind Stress and Drag Coefficient from Spaceborne SAR", Progress in Natural Science, 11, 397-400, 2001.